Applied Physics A (2023) 129:228
https://doi.org/10.1007/s00339-023-06500-9

Applied Physics A
Materials Science & Processing

Microstructure, residual stress, and nanoindentation properties of GCr15-bearing steel by cryogenic treatment and laser-peening composite strengthening

Aixin Feng[1,2,3] · Bingjie Liu[1,2,3] · Yacheng Wei[1,2,3] · Guoxiu Xu[1,2,3] · Chunlun Chen[1,2,3] · Xiaoming Pan[1,3]

Received: 28 September 2022 / Accepted: 14 February 2023 / Published online: 1 March 2023

Abstract
GCr15-bearing steel is widely used in generator bearings. To improve its mechanical properties, the cryogenic treatment and laser-peening (CT + LP) composite strengthening process and properties of GCr15-bearing steel were studied in this paper. The microstructure, residual stress distribution and nanoindentation properties of GCr15-bearing steel under CT + LP composite strengthening were studied by X-ray diffraction, scanning electron microscope, transmission electron microscope, X-ray stress analyzer and nanoindentation instrument. The experimental results showed that the residual compressive stress value and FWHM (full width at half maximum) value of the surface of GCr15-bearing steel increased after CT + LP composite strengthening, and the microstructure characteristics such as dislocation entanglement, proliferation, subgrain boundary and nanocrystalline appeared inside the CT + LP specimen. The nano-hardness and elastic modulus of CT + LP sample were 6.55 and 221.95 GPa, respectively, which were 12.94% and 32.61% higher than that of the untreated sample, respectively. The nanoindentation properties and deformation resistance of GCr15-bearing steel were improved.

Keywords GCr15-bearing steel · CT + LP · Microstructure · Residual stress · Nanoindentation properties

1 Introduction

Bearings are one of the core basic components of the machinery industry, and are the basis for the survival and development of modern industries [1–3]. The generator bearing is mainly made of GCr15-bearing steel. GCr15 is a high-carbon chromium-bearing steel with less alloy content, high hardness, uniform structure, good comprehensive performance and the most extensive application. In harsh service conditions, such as sand and rain, there are wear, fatigue and corrosion failure problems. At present, there are two main ways to strengthen bearings, which are divided into surface modification and overall modification. The surface modification includes surface heat treatment, mechanical strengthening, and high-energy surface treatment. Integral modification allows the bearing to be cryogenically treated. Although these two methods can alleviate the wear to a certain extent, the modification treatment of a single method has the shortcomings of shallow residual stress layer, difficult to precisely control and insignificant strengthening effect. Therefore, it is a good method to consider the effective coupling of bulk modification and surface strengthening to improve material properties.

Cryogenic treatment (CT) is a strengthening method that treats the material as a whole and improves the mechanical properties of the material. CT can improve the wear resistance of materials [4–7], enhance the dimensional stability of parts and prolong their service life [8], the modification effect is lasting, the operation is simple, and there is no pollution [9]. Çakir [10] et al. performed shallow (− 80 °C) and deep (− 196 °C) low temperature treatments on Ti6Al4V alloys, and the study showed that with the application of low temperature treatment, the internal structure of the material changed, and after 36 h with the CT, the β phase ratio of the alloy decreased from 8.1% to 5.6%. The unstable β phase

✉ Yacheng Wei
20451438039@stu.wzu.edu.cn

[1] College of Mechanical and Electrical Engineering, Wenzhou University, Wenzhou 325035, China

[2] Ruian Graduate College, Wenzhou University, Ruian 325000, China

[3] Zhejiang Provincial Key Laboratory of Laser Processing Robots/Machinery Industry Key Laboratory of Laser Processing and Testing, Wenzhou 325035, China

transformed into α phase and stable β phase, in addition to improving the plasticity and toughness of Ti6Al4V alloy at room temperature. Although CT can improve the wear resistance of the material, the toughness of the material will be reduced at the same time, which reduces the gain effect of the wear resistance of the bearing. Due to its unique advantages, laser-peening (LP) [11–14] technology has attracted extensive attention in the field of material surface engineering. The metal material is irradiated with high power density pulse energy to form a plasma-peening wave to the surface of the material. The internal radiation of the material, under the action of the peening wave, produces a high-amplitude residual stress [15, 16], forms a high-density dislocation structure, improves the internal microstructure of the material [17–21], and enhances the wear resistance of metal materials. Fatigue and corrosion resistance properties. Therefore, some researchers combined cryogenic treatment and laser peening to strengthen the material, and obtained some beneficial conclusions. Ye et al. [22] performed laser shock peening (LSP) on 304 stainless steel at room temperature and cryogenic temperature (liquid nitrogen temperature), the results showed that cryogenic temperature laser shock peening (CLSP) produced a higher volume fraction of martensite than room temperature laser shock peening (RT-LSP) at the same laser intensity. In addition, CLSP generated a high density of deformation twins and stacking faults, and the combined effect of higher surface hardness and a more stabilized microstructure resulted in greater fatigue performance improvement of the CLSP samples. Li et al. [23] explored the effects of room temperature laser peening (RT-LP) and cryogenic laser peening (CLP) on the microstructural characteristics and microhardness of pure titanium (Ti), the results showed that compared with RT-LP, the microhardness improvement caused by CLP was higher, and CLP induced higher density of mechanical twins and dislocation structures.

At present, there is no report on the nanoindentation properties of GCr15-bearing steel through CT + LP composite strengthening. In this paper, the microstructure evolution and nanoindentation properties of GCr15-bearing steel induced by CT + LP composite strengthening were investigated using GCr15-bearing steel as the research material, and the improvement mechanism of GCr15-bearing steel modification under the coupling effect of CT + LP composite strengthening was revealed. These findings provide theoretical references for the strengthening of GCr15-bearing steel in the manufacturing industry.

2 Experimental procedures

2.1 Material and experimental setup

The test material was GCr15-bearing steel, and the chemical composition is shown in Table 1. The size of the sample was 40 mm × 30 mm × 4 mm (length × width × thickness), and its surface was polished with 320 #–2000 # water sandpapers step by step, and then the sample was immersed in acetone solution for cleaning to remove adhesion contamination on the sample surface. Finally, the samples were placed in an ultrasonic cleaner and rinsed with deionized water by ultrasonic vibration.

The experiments were grouped into four groups: untreated, CT treatment, LP treatment, and CT + LP composite treatment. The experimental procedures for different processing are shown in Table 2. The specific procedure of CT + LP composite treatment was to carry out CT first, and then carry out LP treatment. According to the previous experiments, the CT environment was set to a liquid nitrogen environment of − 196 °C, and the cryogenic time was 9 h. The LP test was carried out on the SIA-LSP-21 laser-peening wave equipment system. The schematic diagram of LP is shown in Fig. 1. The laser process parameters were: wavelength 1064 nm, pulse width 15 ns, repetition frequency 2 Hz, light spot diameter 3 mm, pulse energy 10 J, the number of laser peening was three times (pulsed laser emission for a period of time, 3 times in a row), the overlap rate of light spot was 50%. The flow water with a thickness of 2 mm was used as the constraining layer of LP, and the special aluminum foil of 0.1 mm was selected as the laser energy absorption layer, which could protect the workpiece from loss by laser ablation and enhance the absorption of laser energy.

Table 2 Experimental groups of different process treatments

Experimental groups	CT procedure	LP procedure
Untreated	/	/
CT	− 196 °C, 9 h	/
LP	/	1064 nm, 10 J, 15 ns, 3 times
CT + LP	− 196 °C, 9 h	1064 nm, 10 J, 15 ns, 3 times

Table 1 Chemical composition of GCr15-bearing steel (wt%)

C	Cr	Mn	Si	S	P	Fe
0.95–1.05	1.30–1.37	0.20–0.40	0.15–0.35	≦ 0.02	≦ 0.027	Balance

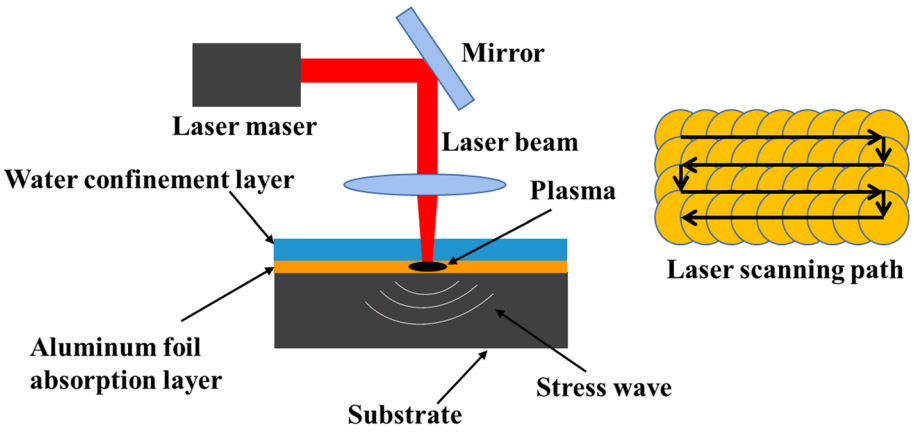

Fig. 1 Schematic diagram of laser peening

2.2 Characterization *methods*

The samples treated with different processes were cut into block samples with a size of 10 mm × 10 mm × 4 mm by a wire cutting machine, and a BRUKER D8 ADVANCE X-ray diffractometer (XRD) was used to investigate the variation of the material phase in different specimens, The Cu target was selected as the X-ray source of the experiment, and the scanning angle range was set to 20°–90°, and the scanning speed was set to 5°/min.

The samples were ground and polished step by step, ultrasonically cleaned and then dried. The surface to be tested was corroded with 4% nitric acid for 30 s, and then ultrasonically cleaned and dried. The TESCAN VEGA3 scanning electron microscope (SEM) was used to observe the microstructure and precipitation phase of GCr15-bearing steel, and a matched energy dispersive spectrometer (EDS) was used for elemental analysis.

The FEI Talos F200X transmission electron microscope (TEM) was used to further characterize the microstructure of GCr15-bearing steel. The sample was cut into thin slices of about 0.5 mm by wire cutting technology, and the untreated surface was polished with sandpaper of different meshes. The sample was mechanically thinned to a thickness of 50 μm and then ionically thinned to produce a TEM sample. During the processing, the sample shall not be warped to avoid introducing internal stress, and selected area electron diffraction (SAED) was performed on the relevant regions to analyze the evolution characteristics of dislocation configuration in different samples.

The LXRD X-ray diffraction stress analyzer of PROTO company was used to analyze the residual stress of GCr15-bearing steel and the distribution law of FWHM. The X-ray tube used was Cr_K-Alpha, the tube voltage and tube current were 30 kV and 25 mA, respectively, and the Bragg angle was 156°, Beta rocking 3°, Phi rocking 0°. An aperture of 1 mm in diameter was selected, the exposure time was 1 s, and the number of exposures was 10 times. During the measurement, measure every 1 mm on the surface of each sample, and test 5 points in total, and then took the average value as the residual stress value on the surface of the GCr15-bearing steel samples.

The nano-hardness and elastic modulus of the sample surface were measured by HysitronTi950 nanoindentation instrument to characterize the nanoindentation properties of specimens. The maximum load of the nanoindentation test was 1000 μN, and the pressure holding time was 10 s. During the test, a point is measured every 50 μm, a total of 10 points are measured, and then the average value was calculated as the result of nano-hardness and elastic modulus of the final sample.

3 Results and discussion

3.1 Phase analysis

Figure 2 presents the XRD quantitative refinement diagrams of different samples. Cal, Obs, and Cal-Obs in the figure indicate the calculated results, experimental observations, and deviation of the fitted curve, respectively, and Rwp indicates the degree of deviation after refinement of the XRD diagram. It can be seen from Fig. 2 that after CT, LP and CT + LP composite strengthening, GCr15-bearing steel would not produce excess phases. The main phases of each specimen were Fe_3C and Fe_4C in addition to martensite and austenite.

To further analyze the effect of CT + LP composite strengthening on the retained austenite content in the material, the residual austenite content of each sample was extracted as shown in Table 3. The residual austenite content of the untreated sample was 1.5%, and after CT, the residual austenite content in the CT sample was reduced to 0.81%, a decrease of 46%. After LP, the residual austenite content decreased to 1.08%, a decrease of 28%. The residual austenite content of the CT + LP sample was 0.42%, which

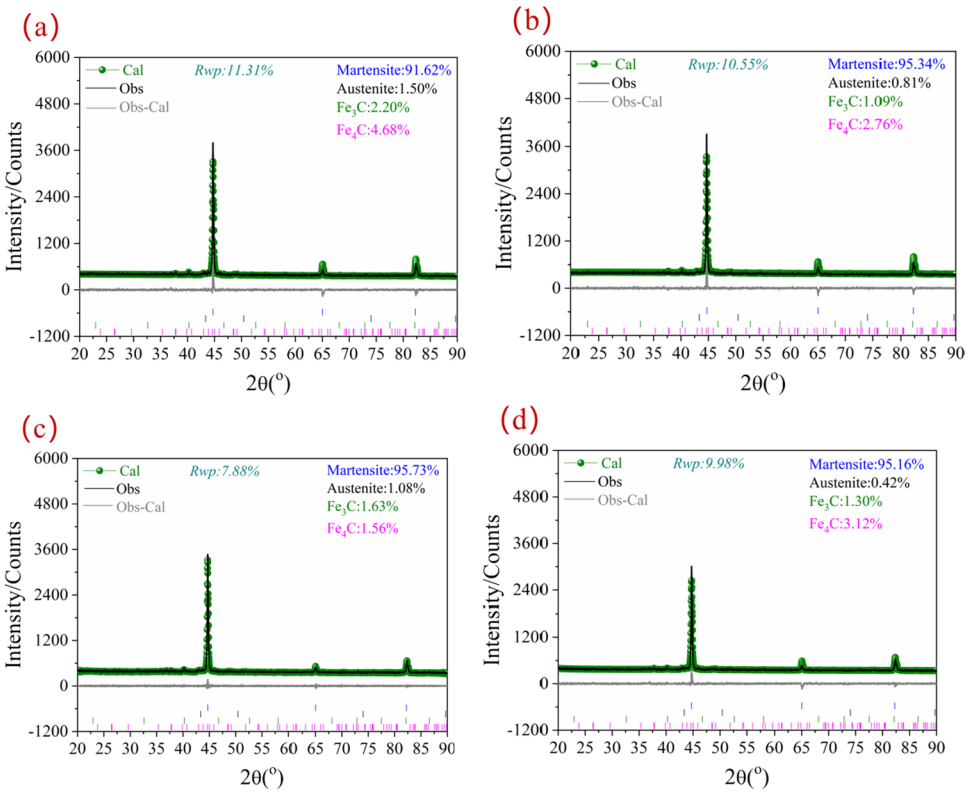

Fig. 2 XRD quantitative refinement analysis of samples treated with different processes. **a** Untreated, **b** CT, **c** LP, **d** CT + LP

Table 3 Residual austenite content of samples with different treatments

Samples	Untreated	CT	LP	CT + LP
Residual austenite content (%)	1.5	0.81	1.08	0.42

was 72% lower than that of the untreated sample and 59.26% lower than that of the LP sample. This was mainly due to the coupling effect of CT and LP, the residual austenite in the specimen was further transformed into martensite, which reduced the content of residual austenite in the specimens. The CT + LP specimen had the lowest residual austenite content, which is beneficial to the performance improvement of GCr15-bearing steel [24].

3.2 Microstructure analysis

Figure 3 demonstrates the surface SEM images of different specimens, and it can be seen that there were some black granular precipitates on the surface of each specimen, the precipitated phase of the untreated specimen in Fig. 3a is lower. Whether after CT or LP, more precipitation phases appeared on the surfaces of both CT and LP specimens, as shown in Fig. 3b, c, respectively. In addition, it is obvious from Fig. 3d that the precipitation phases on the surface of GCr15-bearing steel were more and more uniformly distributed after CT + LP composite strengthening. To further investigate the elemental composition of the precipitated phase, the energy spectrometer (EDS) was used to test the energy spectrum of point A in Fig. 3d, and the analysis results showed that the precipitated phase was mainly composed of C and Fe elements. This is consistent with the conclusion in Fig. 2 that the precipitated secondary phases were mainly Fe_3C and Fe_4C.

To further analyze the effect of CT + LP composite strengthening on the microstructure of GCr15-bearing steel, the TEM images of the untreated specimen and CT + LP specimen are shown in Fig. 4. It can be seen from Fig. 4a that some dislocation lines were dispersed in the original tissue of the untreated sample. After GCr15-bearing steel undergone CT + LP composite strengthening, a large number of microstructures such as dislocation entanglements, dislocation cells, and subgrain boundaries were distributed on its surface, as shown in Fig. 4b–e. Figure 4f shows the selected area electron diffraction (SAED) pattern at the circle in Fig. 4e. It could be seen that the arrangement of the spots in the figure was very regular, and the diffraction intensity of each spot was not equal, so we could judge that this was a single crystal electron diffraction image. Combined with the microscopic scale of this region, the analysis indicated that CT + LP composite strengthening promoted the formation of small-sized single crystal structures, refined the grains of GCr15-bearing steel.

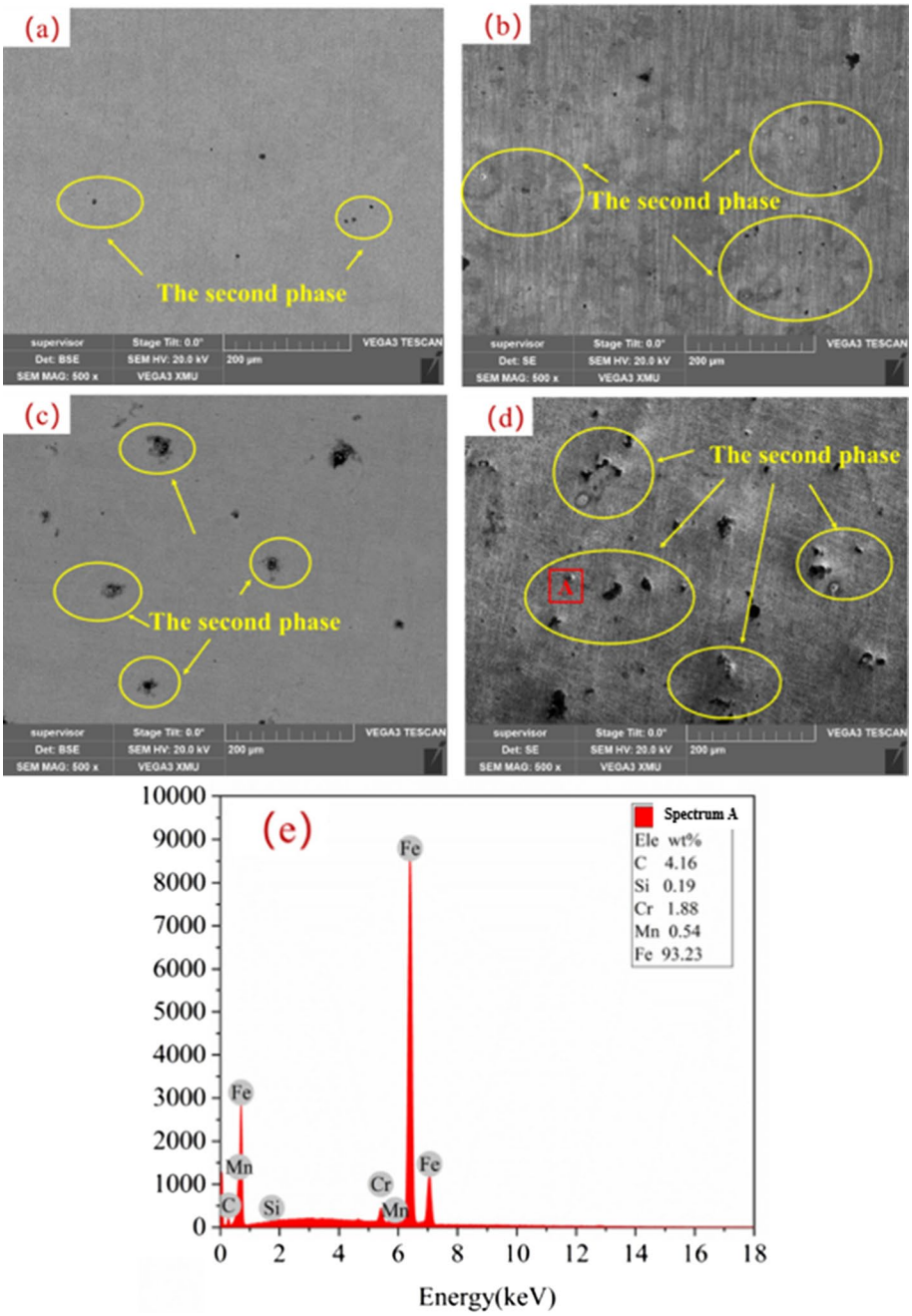

Fig. 3 Surface SEM images of samples treated with different processes **a** untreated, **b** CT, **c** LP, **d** CT + LP, **e** energy spectrum of precipitate phase at point A

After CT + LP composite strengthening, the ultra-low temperature [25] of CT caused the material to shrink in volume, followed by plastic deformation of the surface layer of GCr15-bearing steel under the radiation of laser shock waves, which promoted the generation, movement and proliferation of dislocations. Different dislocation motions leaded to the generation of dislocation walls and dislocation entanglements on the surface of GCr15-bearing steel. When the dislocation density reached a certain value, the dislocation structure would annihilate and rearrange. At this time, to balance the internal energy of the system, the dislocations were further developed into dislocation cells. Moreover, under the synergistic strengthening effect of ultra-low temperature and laser shock wave, the GCr15-bearing steel further undergone plastic deformation, which made the dislocation cells evolve into subgrains, and finally, the subgrains evolved into grains, causing the grains refinement of the GCr15-bearing steel. In addition, the cryogenic temperature in the process of CT + LP composite strengthening could inhibit the dynamic recovery and annihilation of dislocations. At the same time, due to the volume shrinkage effect of GCr15-bearing steel, the precipitation of solute atoms was accelerated. The interaction between the solute atoms and the dislocation structure generated by LP forms the Cottrell

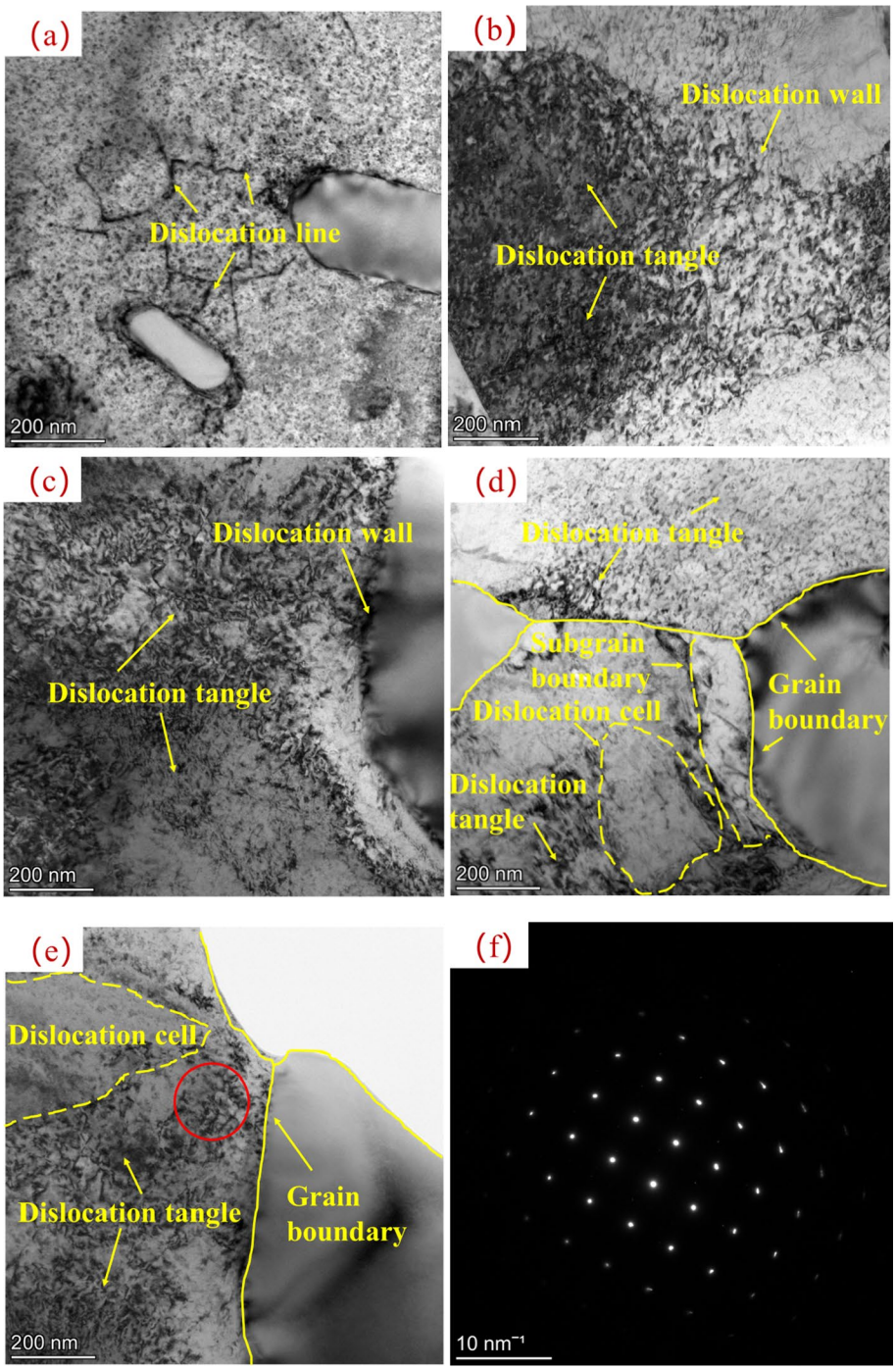

Fig. 4 TEM images of untreated and CT + LP specimens, **a** untreated, **b**–**e** CT + LP, **f** SAED pattern of circle in **e**

atmosphere, and the precipitation of the solute atoms could pin the dislocations [26], thus hindering the annihilation of the dislocations and protecting the stability of the dislocation structure.

3.3 Residual stress and FWHM

Figure 5 demonstrates the average residual stress on the surface of different samples. It can be seen from Fig. 5 that the surface residual stress of the untreated specimen was − 53.62 MPa, and the surface residual stress after LP was − 322.78 MPa, an increase of 501.98% compared with the untreated sample. After CT, the residual stress on the surface of the material increased to − 220.62 MPa compared with the untreated sample, an increase of 311.45%. In addition, GCr15-bearing steel could be induced to generate higher amplitude residual compressive stress after CT + LP composite strengthening, and the surface residual stress values

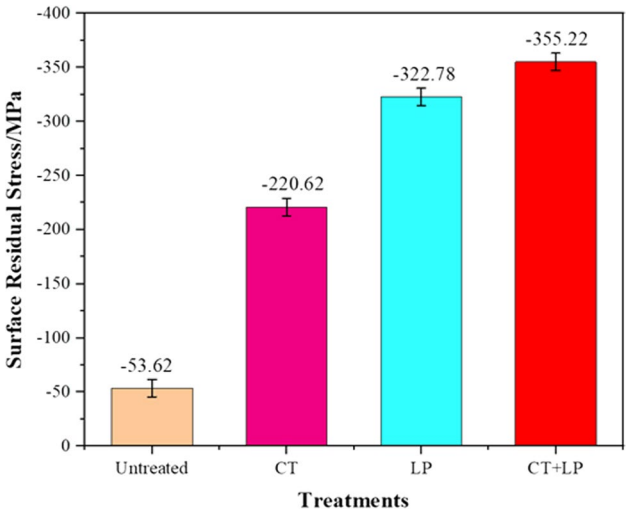

Fig. 5 Surface residual stress values of samples treated with different processes

of CT + LP specimen was increased by 562.48%, 61.01% and 10.05% compared with untreated specimen, CT specimen and LP specimen, respectively, indicating that the CT + LP composite strengthening caused the material surface to generate higher residual compressive stress.

The FWHM values of different sample surfaces are presented in Fig. 6. The FWHM value of the untreated sample was 1.784°, and the FWHM value of the surface of the LP sample after LP was 1.982°, which was 11.1% higher than that of the untreated sample. After CT, the FWHM value increased to 1.883° compared with the untreated sample, an increase of 5.55%. The FWHM value of CT + LP specimen was 2.105°, which was 17.99% higher than that of the untreated sample, and 6.20% higher than that of the LP sample. Under the action of laser shock wave, severe plastic deformation occurred on the surface of GCr15-bearing steel, which promoted the proliferation of dislocations, increased the dislocation density of GCr15-bearing steel, and increased the FWHM value of the material.

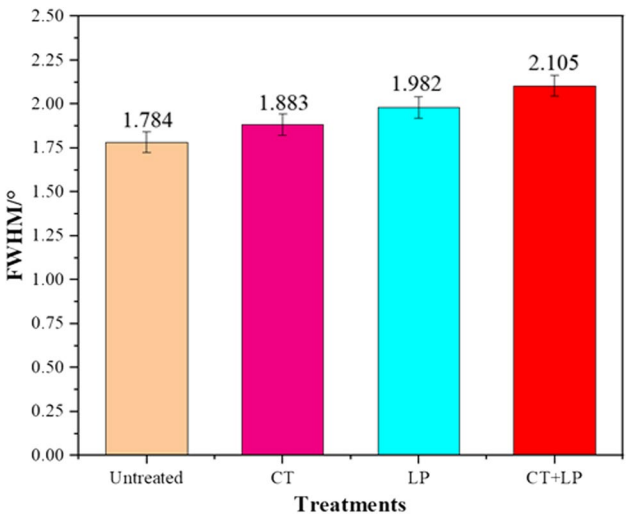

Fig. 6 FWHM values of samples treated with different processes

3.4 Nano-hardness and elastic modulus

Figure 7 presents the nanoindentation displacement load curves of different samples. It can be seen that with the continuous increase of the applied load, the displacement increased continuously. The nano-indentation curves on the surfaces of CT and LP samples had the characteristic of shifting to the left no matter whether it was CT treatment or LP treatment. In addition, after the CT + LP composite strengthening, the surface nano-indentation curve was further leftward. The result showed that both CT and LP can improve the nano-hardness of the surface of GCr15-bearing steel, and the improvement of the nano-hardness of the material surface was more significant after the composite strengthening of CT + LP.

Figure 8 presents the comparison results of the nano-hardness in the surface direction of the samples with different processes. It can be seen that the nano-hardness of the untreated sample was 3.09 GPa. After CT, the surface nano-hardness increased to 3.49 GPa, which was 12.94% higher than that of the untreated specimen. After LP, the surface nano-hardness of the LP specimen increased to 4.88 GPa, which was 57.93% higher than that of the untreated specimen, and 39.83% higher than that of the CT specimen. The surface nano-hardness of the CT + LP specimen was further increased to 6.55 GPa, which was 111.98%, 87.68% and 34.22% higher than that of the

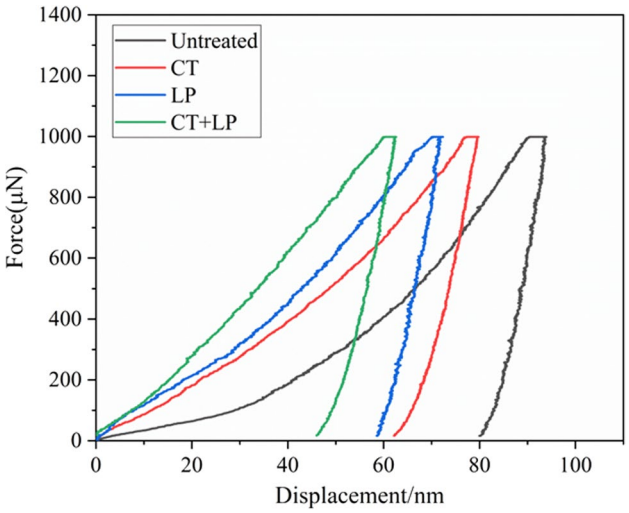

Fig. 7 Nano-indentation displacement–load curves of specimens treated by different processes

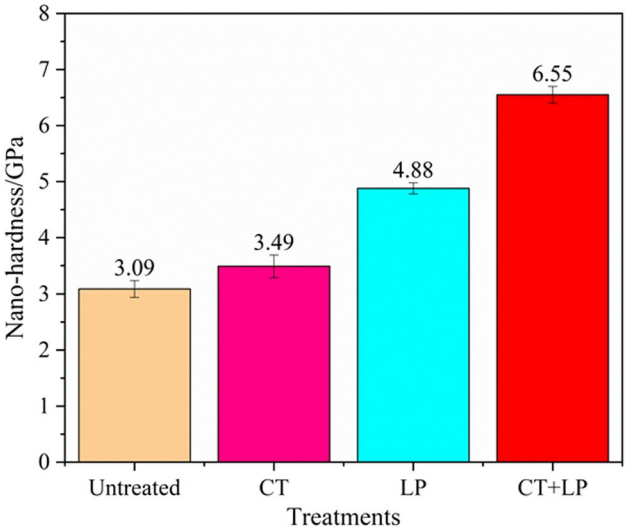

Fig. 8 Nano-hardness of specimens treated by different processes

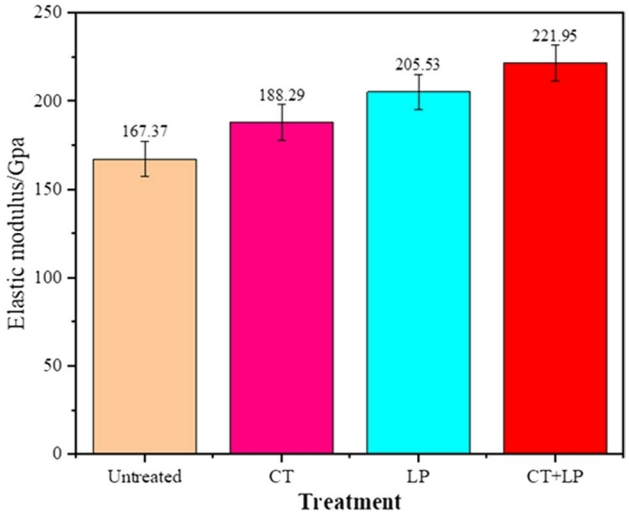

Fig. 9 Modulus of elasticity of specimens treated by different processes

untreated specimen, the CT specimen and the LP specimen, respectively. It could be seen that both CT and LP effectively improve the surface nano-hardness of GCr15-bearing steel, and after CT + LP composite strengthening, the surface nano-hardness of GCr15-bearing steel has been further improved, indicating that CT + LP composite strengthening had more significant effect on the gain of nano-hardness. The analysis showed that under the coupling effect of the ultra-low temperature of CT and the ultra-high strain rate of LP, GCr15-bearing steel undergone volume shrinkage, the retained austenite was further transformed into martensite, and the surface grains of GCr15-bearing steel were finer. High-density dislocation structure was induced, which was beneficial to increase the nano-hardness of the GCr15-bearing steel.

The elastic modulus is one of the important evaluation indicators of material properties, which measures the deformation resistance of the material. Figure 9 demonstrates the variation law of the elastic modulus of the samples with different treatments in the surface direction. It can be seen that the surface elastic modulus of the untreated, CT, LP and CT + LP samples were 167.37 GPa, 188.29 GPa, 205.53 GPa and 221.95 GPa, respectively. Compared with the untreated sample, the surface elastic modulus of CT, LP and CT + LP samples increased by 12.50%, 22.80% and 32.61%, respectively. Compared with the CT and LP samples, the CT + LP sample increased by 17.88% and 7.99%, respectively. It could be seen that after composite strengthening of CT + LP, the surface elastic modulus of GCr15-bearing steel increased more greatly, indicating that the elastic modulus of GCr15-bearing steel has been significantly improved. The effect of composite strengthening of CT + LP on elastic modulus was more significant.

CT + LP composite strengthening couped the characteristics of CT and LP. The volume shrinkage effect caused by cryogenic temperature could generate large internal stress inside the material, which in turn causes the proliferation of a large number of dislocation structures. In addition, due to irradiation of laser shock waves, high-amplitude residual stress was induced on the surface of GCr15-bearing steel, formed a high-density dislocation structure. The dislocations were entangled with each other and precipitate phase pinned dislocations, thus hindering the slip and movement of dislocations, refining the grains [27], which improved the plastic deformation resistance of GCr15-bearing steel.

4 Conclusions

In this study, composite strengthening of CT + LP were used to refine the microstructure and enhance the nanoindentation properties of GCr15-bearing steel, and the effects of CT + LP composite strengthening on phase, residual stress and FWHM, microstructure, nano-hardness and elastic modulus were studied. The main conclusions are as follows:

1. CT + LP composite strengthening would not cause excess phases of GCr15-bearing steel, in addition to martensite and austenite, its phases were mainly Fe_3C and Fe_4C, and the content of residual austenite would be significantly reduced after CT + LP composite treatment but would not be completely eliminated.
2. After composite strengthening of CT + LP, the microstructure analysis showed that a large number of dislocation entanglements, dislocation cells, subgrain boundaries and other microstructures appeared inside the

CT + LP specimen, the analysis indicated that CT + LP composite strengthening promoted the formation of small-sized single crystal structures, refined the grains of GCr15-bearing steel. The phase could pin dislocations, thus hindering the movement and annihilation of dislocations.

3. CT + LP composite strengthening induced large residual compressive stress and FWHM value on the surface of GCr15-bearing steel, which reached − 355.22 MPa and 2.105°, respectively. In addition, through the analysis of nanoindentation characteristics, after CT + LP composite treatment, the nano-hardness and elastic modulus of GCr15-bearing steel were 6.55 GPa and 221.95 GPa, respectively, which were increased by 12.94% and 32.61%, respectively, compared with the untreated sample, which improved the nanoindentation properties and deformation resistance of GCr15-bearing steel.

Author contribution AF: methodology, investigation, writing—original draft preparation, writing—review and editing, BL: methodology, investigation, writing—original draft preparation, YW: data curation, writing—review and editing, GX: conceptualization, methodology, writing—review and editing, CC: methodology, data curation. XP: data curation.

Funding This work was funded by the Wenzhou Science and Technology Bureau Major Science and Technology Special Project (ZG2019002), the Zhejiang Provincial Natural Science Foundation of China (LY20E050027), the Innovation Fund of Wenzhou University Rui'an Graduate College (YC202212010), and the Innovation Fund of Wenzhou University Rui'an Graduate College (YC202212023).

Availability of data and material All data generated or analysed during this study are included in this published article (and its supplementary information files).

Declarations

Conflict of interest The authors have no relevant financial or non-financial interests to disclose.

Ethics approval Not applicable.

Consent to participate The authors agree to participate.

Consent for publication The authors agree to publish.

References

1. H.K.D.H. Bhadeshia, Prog. Mater Sci. **57**, 268 (2012)
2. F. Yu, X.P. Chen, H.F. Xu, H. Dong, Y.Q. Weng, Y.Q. Cao, Acta Metall. Sin. **56**, 513 (2020)
3. Y.H. Wang, Z.N. Yang, F.C. Zhang, Y.M. Qin, Q.B. Wang, B. Lv, Mater. Sci. Eng. A Struct. Mater. Prop. Microstruct. Process. **777**, 139086 (2020)
4. A. Bensely, A. Prabhakaran, D.M. Lal, G. Nagarajan, Cryogenics **45**, 747 (2005)
5. V.I. Bolobov, B. Thanh, IOP Conf. Ser. Mater. Sci. Eng. **327**, 331 (2018)
6. A.R. Rauf Jamali, W. Khan, A.D. Chandio, Z. Anwer, M. Hayat Jokhio, Mehran Univ. Res. J. Eng. Technol. **38**, 755 (2019)
7. B. Podgornik, I. Paulin, B. Zajec, S. Jacobson, V. Leskovsek, J. Mater. Process. Technol. **229**, 398 (2016)
8. B. Bist, Int. J. Pure Appl. Math. **116**, 113 (2017)
9. T. Sonar, S. Lomte, C. Gogte, Mater. Today Proc. **5**, 25219 (2018)
10. F.H. Çakir, O.N. Çelik, J. Mater. Eng. Perform. **29**, 6974 (2020)
11. S. Prabhakaran, S. Kalainathan, P. Shukla, V.K. Vasudevan, Opt. Laser Technol. **115**, 447 (2019)
12. L.M. Kukreja, J.S. Hoppius, K. Elango, M.M. Barrientos, F. Pohl, F. Walther, E. Gurevich, A. Ostendorf, Laser Appl. Mag. **33**, 042048 (2018)
13. A. Siddaiah, B. Mao, Y.L. Liao, P.L. Menezes, Surf. Coat. Technol. **351**, 188 (2018)
14. L. Liu, J.J. Wang, J.Z. Zhou, Vacuum **148**, 178 (2018)
15. T. Kawashima, T. Sano, A. Hirose, S. Tsutsumi, K. Masaki, K. Arakawa, H. Hori, J. Mater. Process. Technol. **262**, 111 (2018)
16. W. Li, Y.H. Li, W.F. He, Q.P. Li, Adv. Laser Optoelectron. **12**, 15 (2008)
17. B.P. Fairand, B.A. Wilcox, W.J. Gallagher, D.N. Williams, J. Appl. Phys. **43**, 3893 (1972)
18. J.Z. Lu, K.Y. Luo, F.Z. Dai, J.W. Zhong, L.Z. Xu, C.J. Yang, L. Zhang, Q.W. Wang, J.S. Zhong, D.K. Yang, Mater. Sci. Eng. A **536**, 57 (2012)
19. M.Z. Ge, J.Y. Xiang, Y. Tang, X. Ye, Z. Fan, Y.L. Lu, X.H. Zhang, Surf. Coat. Technol. **337**, 501 (2018)
20. J.Z. Lu, K.Y. Luo, Y.K. Zhang, C.Y. Cui, G.F. Sun, J.Z. Zhou, L. Zhang, J. You, K.M. Chen, J.W. Zhong, Acta Mater. **58**, 3984 (2010)
21. X.C. Zhang, Y.K. Zhang, J.Z. Lu, F.Z. Xuan, Z.D. Wang, S.T. Tu, Mater. Sci. Eng. A **527**, 3411 (2010)
22. C. Ye, S. Suslov, D. Lin, G.J. Cheng, Philos. Mag. **92**, 1369 (2012)
23. J. Li, J.Z. Zhou, A.X. Feng, Y. Huang, X.H. Tian, S. Huang, X.K. Meng, Opt. Laser Technol. **120**, 105763 (2019)
24. J. Pechousek, L. Kouril, P. Novak, J. Kaslik, J. Navarik, Measurement **131**, 671 (2019)
25. S.H. Li, L.H. Deng, X.C. Wu, Cryogenics **50**, 433 (2010)
26. J. Corrochano, J.C. Walker, M. Lieblich, J. Ibanez, W.M. Rainforth, Wear **270**, 658 (2011)
27. S.J. Lee, J. Kim, S.N. Kane, S.N. Kane, B.C. De Cooman, Acta Mater. **59**, 6809 (2011)